

# Tensor product algorithms for inference of contact network from epidemiological data\*

Sergey Dolgov<sup>†</sup> and Dmitry Savostyanov<sup>‡</sup>

26<sup>th</sup> January 2024

## Abstract

We consider a problem of inferring contact network from nodal states observed during an epidemiological process. In a black-box Bayesian optimisation framework this problem reduces to a discrete likelihood optimisation over the set of possible networks. The high dimensionality of this set, which grows quadratically with the number of network nodes, makes this optimisation computationally challenging. Moreover, the computation of the likelihood of a network requires estimating probabilities of the observed data to realise during the evolution of the epidemiological process on this network. A stochastic simulation algorithm struggles to estimate rare events of observing the data (corresponding to the ground truth network) during the evolution with a significantly different network, and hence prevents optimisation of the likelihood. We replace the stochastic simulation with solving the chemical master equation for the probabilities of all network states. This equation also suffers from the curse of dimensionality due to the exponentially large number of network states. We overcome this by approximating the probability of states in the Tensor-Train decomposition. This enables fast and accurate computation of small probabilities and likelihoods. Numerical simulations demonstrate efficient black-box Bayesian inference of the network.

*Keywords:* epidemiological modelling, networks, tensor train, stochastic simulation algorithm, Markov chain Monte Carlo, Bayesian inference

2020 MSC: 15A69, 34A30, 37N25, 60J28, 62F15, 65F55, 90B15, 95C42

## 1 Introduction

The recent outbreak of COVID-19 and the public discussion that followed has led to better understanding of the central role that epidemiological models play in the decision making process and developing an informed response strategy. The quality of the mathematical models used in this process is crucial, not only because it allows to accurately predict the spread of a disease in population, but also in order to increase public trust in research and the decisions that follows from it. The limitations of the the over-simplified homogeneous models [48] in describing the human communities are well understood. To move beyond

---

\*Equal contributions. The order of authors is alphabetical. S.D. was supported by the Engineering and Physical Sciences Research Council New Investigator Award EP/T031255/1. D.S. was supported by the Leverhulme Trust Research Fellowship RF-2021-258.

<sup>†</sup>University of Bath, Claverton Down, Bath, BA2 7AY, United Kingdom, S.Dolgov@bath.ac.uk.

<sup>‡</sup>University of Essex, Wivenhoe Park, Colchester, CO4 3SQ, United Kingdom, D.Savostyanov@essex.ac.uk, dmitry.savostyanov@gmail.com.

the Kermack–McKendrick compartmental SIR model [48], we should discard the assumption that population is ‘well-mixed’ and include the information on the structure of contact network, leading to study of epidemics on networks [47, 13, 75, 62, 49].

Predicting the evolution of epidemic on a given network is much more difficult than solving a homogeneous model. If the number of individuals assigned to each network node is small (which is the most interesting alternative to homogeneous models), the evolution becomes stochastic, and one needs to model a probability distribution function of states instead of states themselves. This probability distribution function satisfies the chemical master equation (CME) [71], which is an ordinary differential equation on the probability values. However, the total number of network states (and hence the size of the CME) grows exponentially in the number of network nodes [13, 75]. This makes the direct solution of the stochastic network models computationally intractable for large networks [49].

Perhaps the most traditional method for tackling the CME is the Stochastic Simulation Algorithm (SSA) [29] and variants, which compute random walks over the network states, distributed according to the CME solution. However, as a Monte Carlo method, the SSA is known to converge slowly, especially for rare events. Alternative approaches include mean-field approximations [46, 63], effective degree models [31, 52, 70], and edge-based compartmental models [56], but these models are approximate and rely on truncation of the state space. This introduces a truncation error that is difficult to estimate and/or keep below a desired tolerance for a general network. Other approaches include changing the original model into a surrogate model such as birth–death processes [17], or using neural networks [34, 69]. For solving the original model in a numerically controllable approximation framework, a new approach based on tensor product factorisations was recently proposed by authors in [21].

If the contact network is not known, we can attempt to solve an inverse problem, i.e. to infer the network from observations of disease data over time. For  $N$  network nodes, the number of possible networks grows exponentially in  $N^2$ . Hence, for large  $N$ , the problem complexity typically grows much faster than the information available, and network inference becomes a (very) underdetermined problem [16]. Network inference is therefore only solved directly for very small population sizes [59, 24]. Networks with mass-action kinetics can be inferred uniquely by observing transition rates at a simplex set of states [25], but the cardinality of this set is combinatorial in  $N$ .

To address the problem for larger  $N$ , one can involve additional information about the network structure, such as degree distribution and sparsity [57, 35]. In a similar way, one can assume the underlying statistical distribution for the network and infer its parameters [33]. Another approach is to infer properties of the network rather than its exact structure [9], e.g. to find a class of network distributions, which the contact network most likely belongs to [17]. Related work include inferring the origin of epidemic given the contact network [53]. For a recent survey on network inference see [10].

In this paper we investigate inference of the contact network from states of the network observed over time. We use a Bayesian formulation but do not assume any prior knowledge on the structure of the contact network, and thus solve a black-box optimisation problem

$$\text{network}_{\text{opt}} = \arg \max_{\text{network}} \text{P}(\text{data} \mid \text{network}),$$

i.e. look for the optimal network for which the actually observed data are most likely to appear. To summarise the above, the network inference problem is difficult due to the following reasons.

1. Large inverse problem. The inverse problem is a high-dimensional discrete optimisation problem. Indeed, in an undirected network with  $N$  nodes there are  $\frac{1}{2}N(N-1)$  potential links, which are the optimisation variables, each of which can independently be

in one of two states (on/off). In total, the search space which consists of  $2^{N(N-1)/2}$  possible networks, hence the exhaustive search is computationally unfeasible. Since the optimisation variables are discrete, the gradient of the target function is unavailable, and hence we can't apply steepest descend or Newton–Raphson algorithms. Hence, to find the near-optimal solution, we need to explore the structure of the high-dimensional array with some (possibly heuristic) algorithm, which may require a large number of target function evaluations.

2. Large forward problem. For each network in the search space, a single evaluation of the target function requires solving a forward problem, i.e. finding a probability of given data to be observed during the evolution of the disease on the current network. This is a Markov chain problem on the state space of accessible network states, which scales exponentially with the number of nodes, causing the currently available algorithms to struggle.
3. Low contrast caused by insufficient data. We may observe conditional probabilities to be (almost) the same,  $P(\text{data}|\text{network}_1) \approx P(\text{data}|\text{network}_2)$ , for example if the two networks differ only by the links attached to the nodes, for which we do not have (enough) events in the observed dataset. In this case, the Bayesian optimisation won't be able to choose one particular network, as a large number of them are equally likely to produce the observed dataset. Any numerical approximation errors due to limitations of the forward problem solvers (see item 2) add extra noise to the high-dimensional probability density function and further complicate the optimisation process (see item 1). Due to the probabilistic nature of the problem, the ground truth network  $\text{network}_*$ , for which the observed dataset was generated, may differ from the optimal network recovered by the Bayesian inference method,  $\text{network}_* \neq \text{network}_{\text{opt}}$ .
4. High contrast caused by a large amount of data. Although adding more data makes the ground truth network a unique global optimum for Bayesian optimisation, it also creates a large number of local optima. In a black-box optimisation setting, there is no prior information that could navigate the optimisation towards the global optimum, and the algorithm can be trapped in a local optimum for considerable time.

The existing literature often does not consider these issues separately, nor approach the problem directly. It is typically stated that the network optimisation is impossible to solve, and alternative formulations are considered [16, 49, 10, 17]. In this paper we attempt to perform the black-box network inference directly following the Bayesian optimisation framework. To tackle the forward problem, we solve the CME using tensor product factorisations [21]. A related work was recently proposed in tensor network community, but it is limited to linear one-dimensional chains [54]. We demonstrate that the proposed method provides faster and more accurate solution to the forward problem compared to SSA, particularly when the network is far from optimal.

Next, we apply two Markov Chain Monte Carlo (MCMC) algorithms for black-box discrete high-dimensional optimisation and analyse results. An overall workflow of this procedure is illustrated in Figure 1. By simulating three examples of networks, we show that by collecting sufficiently many data we can make the contrast high enough to infer the original ground truth network.

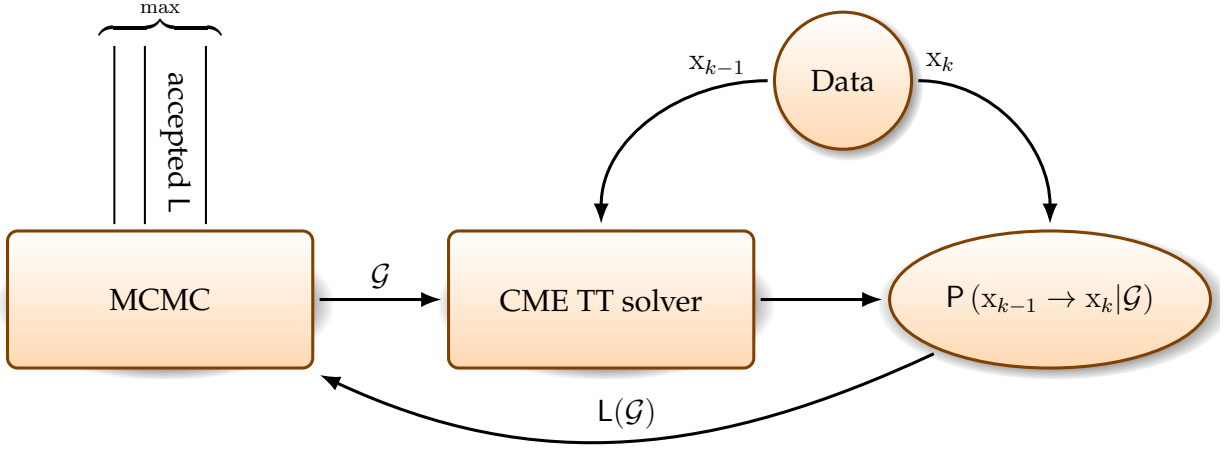


Figure 1: Network inference workflow. An MCMC algorithm samples proposal network configurations,  $\mathcal{G}$ . The CME is solved on each time interval  $[t_{k-1}, t_k]$  in the observed data, starting from the state observation  $X(t_{k-1}) = x_{k-1}$  and obtaining the TT approximation of the probability of observing the state  $X(t_k) = x_k$  for the given network  $\mathcal{G}$ . These probabilities for all data are multiplied to form the likelihood  $L(\mathcal{G})$ , which is accepted or rejected in the MCMC. Finally, the network with the maximum likelihood among the MCMC samples is inferred.

## 2 Methods

### 2.1 Forward problem: $\varepsilon$ -SIS epidemic on network

We consider the  $\varepsilon$ -SIS model of the contact process, which is a variation of a classical susceptible–infected–susceptible (SIS) model, allowing for every node to self-infect with rate  $\varepsilon$ . This process was originally proposed by Hill et al. to describe the spread of emotions in social network [40]. Mieghem et al. studied analytical properties of the model for fully connected networks [72, 1]. Zhang et al. extended this study to arbitrary networks and found conditions under which the equilibrium distribution can be accurately approximated by a scaled SIS process, gaining useful insights on vulnerability of the population [76].

The classical SIS model has an absorbing state where all nodes are susceptible (i.e. the network is fully healthy), but due to spontaneous self-infections the  $\varepsilon$ -SIS model does not have an absorbing state, hence the epidemics lasts forever. This property allows us to observe the epidemics for sufficiently long time and eventually collect the dataset which is large enough to ensure the required contrast for the Bayesian optimisation.

We consider a  $\varepsilon$ -SIS epidemic on a unweighted simple network  $\mathcal{G} = (\mathcal{V}, \mathcal{E})$ , which is a set of nodes (representing people, or agents)  $\mathcal{V} = \{1, 2, \dots, N\}$  and links (or edges, representing contacts between agents)  $\mathcal{E} = \{(m, n) : m \in \mathcal{V}, n \in \mathcal{V}, m \neq n\}$ . We additionally assume that the contacts are bidirectional, i.e.  $(m, n) \in \mathcal{E} \Leftrightarrow (n, m) \in \mathcal{E}$ , which allows us to introduce a symmetric adjacency relation  $m \sim n \Leftrightarrow (m, n) \in \mathcal{E}$  for the connections.

Each node can be in one of two states,  $x_n \in \mathbb{X} = \{\text{susceptible}, \text{infected}\} = \{0, 1\}$ , for  $n \in \mathcal{V}$ . The state of the whole network is therefore a vector  $\mathbf{x} = (x_1 \ x_2 \ \dots \ x_N)^T \in \mathbb{X}^N$ . We consider the system dynamics as a continuous–time Markov jump process on the state space  $\Omega = \mathbb{X}^N$ . The following two types of transitions (or reactions), infection and recovery, occur

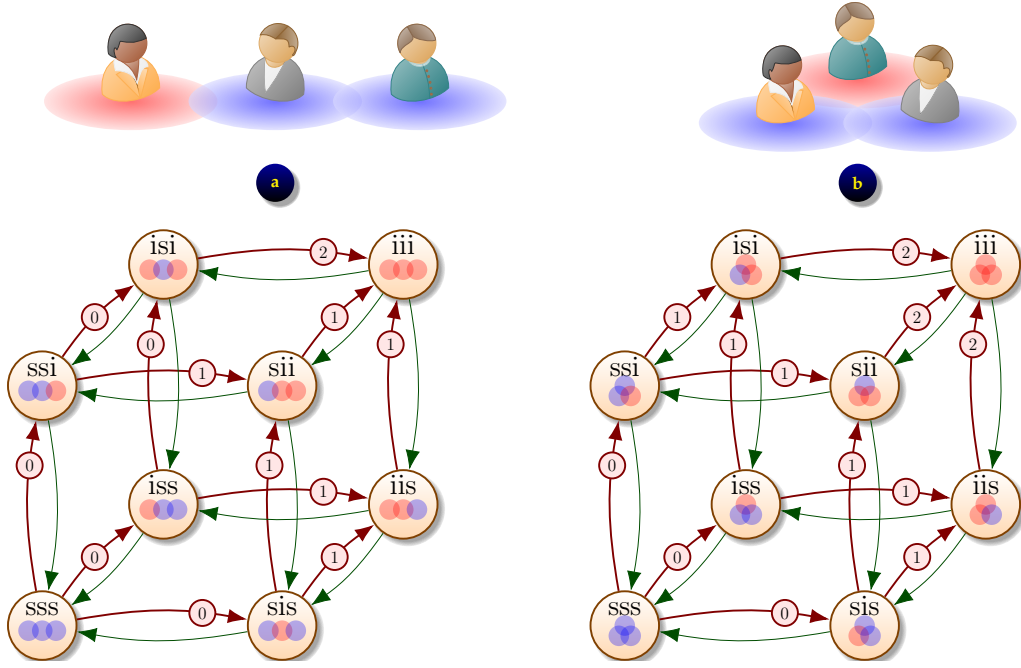


Figure 2: Markov transitions between network states: (a)  $\varepsilon$ -SIS epidemic on a chain of  $N = 3$  people; (b)  $\varepsilon$ -SIS epidemic in a fully connected network of  $N = 3$  people. On the graph, green arrows denote recovery process with rate  $\gamma$ , and red arrows with a circled number  $k$  denote infection process with rate  $k\beta + \varepsilon$ .

independently and at random according to the Poisson process with the following rates

$$p_{x \rightarrow y} = \begin{cases} p_{x \rightarrow y}^{(\text{inf})}, & \text{if } \exists n \in \mathcal{V} : y = x + e_n; \\ p_{x \rightarrow y}^{(\text{rec})}, & \text{if } \exists n \in \mathcal{V} : y = x - e_n; \\ 0, & \text{otherwise,} \end{cases} \quad (1)$$

where  $e_n \in \mathbb{R}^N$  is the  $n$ -th unit vector. For simplicity, we assume that the recovery rates  $p_{x \rightarrow y}^{(\text{rec})} = \gamma$  are the same for all nodes of the network. In the classical SIS model, the infection rate for the susceptible node  $x_n = 0$  is proportional to the number of its infected neighbours,  $I_n(x) = |\{m \in \mathcal{V} : m \sim n, x_m = 1\}|$ , and the per-contact rate  $\beta$ , which we also consider the same across all network. In the  $\varepsilon$ -SIS model, an additional infection rate  $\varepsilon$  is introduced to describe possible infection through contacts with the external, off-the-network, environment. Hence, the infection rate is  $p_{x \rightarrow y}^{(\text{inf})} = I_n(x)\beta + \varepsilon$ . Examples of the Markov transition graph are shown in Fig. 2.

The stochastic properties of the system are described as probabilities of network states  $p(x, t) = \text{P}(\text{system is in state } x \text{ at time } t)$ . The system dynamics is written as a system of ordinary differential equations (ODEs), known as *Markovian master equation* [71, 13], Chapman or *forward Kolmogorov equations*:

$$p'(x, t) = \sum_{y \in \Omega} (p_{y \rightarrow x} \cdot p(y, t) - p_{x \rightarrow y} \cdot p(x, t)), \quad x \in \Omega, \quad (2)$$

subject to initial conditions  $p(x_0, 0) = 1$  for the initial state  $x = x_0$  and  $p(x, 0) = 0$  otherwise. The number of ODEs scales as  $2^N$ , making traditional numerical solvers struggle for even moderate values of  $N$ .

## 2.2 Inverse problem: Bayesian inference of the network

Our goal is to infer the most probable contact network  $\mathcal{G} = (\mathcal{V}, \mathcal{E})$  from the observed data  $\mathcal{X} = \{t_k, \mathbf{x}(t_k)\}_{k=0}^K$ . According to the Bayes theorem [8],  $P(\mathcal{G}|\mathcal{X}) = \frac{P(\mathcal{X}|\mathcal{G})P(\mathcal{G})}{P(\mathcal{X})}$ , where  $P(\mathcal{G})$  is the *prior* probability distribution for the grid,  $P(\mathcal{X}|\mathcal{G})$  is the *likelihood* of the observed data as a function of the grid  $\mathcal{G}$ ,  $P(\mathcal{X})$  is the probability of the observed data, and  $P(\mathcal{G}|\mathcal{X})$  is the posterior probability of the grid given the data.

The connectivity network  $\mathcal{G}$  can be described by its adjacency matrix  $G = [g_{m,n}]_{m,n \in \mathcal{V}}$  with  $g_{m,n} = 1 \Leftrightarrow (m, n) \in \mathcal{E}$  and  $g_{m,n} = 0$ , otherwise. Since  $\mathcal{G}$  is simple,  $G$  is a binary symmetric matrix,  $G = G^T$ , with zero diagonal,  $\text{diag}(G) = 0$ . It is easy to see that a grid  $\mathcal{G}$  can be described by  $\frac{1}{2}N(N-1)$  independent binary variables  $g_{m,n} \in \mathbb{B} = \{0, 1\}$  with  $m, n \in \mathcal{V}$  and  $m > n$ , representing the states (on/off) of possible edges  $(m, n) \in \mathcal{E}$ . Therefore, for a fixed number of nodes  $|\mathcal{V}| = N$ , the set of all possible networks  $\mathbb{G} = \{\mathcal{G} : g_{m,n} = g_{n,m} \in \mathbb{B}, m, n \in \mathcal{V}, m > n\}$  has cardinality  $|\mathbb{G}| = 2^{N(N-1)/2}$ . Note that  $\mathbb{G}$  is isomorphic to  $\mathbb{B}^{N(N-1)/2}$ , the set of adjacency elements  $g_{m,n}$ . The structure of this set is illustrated in Fig. 3.

Assuming that nodes are known and no prior information of the edges  $\mathcal{E}$  is available, we take the uniform prior distribution,  $P(\mathcal{G}) = 2^{-N(N-1)/2}$ . Although  $P(\mathcal{X})$  is unknown, it does not affect the optimisation problem, as  $\max_{\mathcal{G}} P(\mathcal{G}|\mathcal{X}) = \frac{2^{-N(N-1)/2}}{P(\mathcal{X})} \max_{\mathcal{G}} P(\mathcal{X}|\mathcal{G})$ , hence  $\arg \max_{\mathcal{G}} P(\mathcal{G}|\mathcal{X}) = \arg \max_{\mathcal{G}} P(\mathcal{X}|\mathcal{G})$ .

Due to the Markovian property of the system dynamics, the likelihood can be expanded as follows,

$$\begin{aligned} L(\mathcal{G}) &= P(\mathcal{X}|\mathcal{G}) = P(X(t_1) = \mathbf{x}_1, \dots, X(t_K) = \mathbf{x}_K|\mathcal{G}) \\ &= P(X(t_1) = \mathbf{x}_1|X(t_0) = \mathbf{x}_0, \mathcal{G}) \cdots P(X(t_K) = \mathbf{x}_K|X(t_{K-1}) = \mathbf{x}_{K-1}, \mathcal{G}), \\ &= \prod_{k=1}^K \underbrace{P(X(t_k) = \mathbf{x}_k|X(t_{k-1}) = \mathbf{x}_{k-1}, \mathcal{G})}_{P(\mathbf{x}_{k-1} \rightarrow \mathbf{x}_k|\mathcal{G})}, \end{aligned} \quad (3)$$

where  $X(t) \in \mathbb{X}^N$  are random variables describing the network states during its stochastic evolution, and the time sequence  $\{t_k\}_{k=0}^K$  is monotonically increasing. We see that the likelihood is a product of transition probabilities  $P(\mathbf{x}_{k-1} \rightarrow \mathbf{x}_k|\mathcal{G}) = P(X(t_k) = \mathbf{x}_k|X(t_{k-1}) = \mathbf{x}_{k-1}, \mathcal{G})$ , which are the probabilities for the system to evolve from the state  $\mathbf{x}_{k-1}$  to  $\mathbf{x}_k$  over the time period  $[t_{k-1}, t_k]$ . The (black-box) Bayesian network inference therefore boils down to likelihood optimisation,

$$\mathcal{G}_{\text{opt}} = \arg \max_{\mathcal{G} \in \mathbb{G}} \log L(\mathcal{G}) = \arg \max_{\mathcal{G} \in \mathbb{G}} \sum_{k=1}^K \log P(\mathbf{x}_{k-1} \rightarrow \mathbf{x}_k|\mathcal{G}). \quad (4)$$

To compute a single log-likelihood  $\log L(\mathcal{G})$  in (4), we need to solve  $K$  forward problems, i.e. estimate the chance of arriving to the state  $\mathbf{x}_k$  from the state  $\mathbf{x}_{k-1}$  over the period of time  $t \in [t_{k-1}, t_k]$  for  $k = 1, \dots, K$ . To find the optimal network  $\mathcal{G}_{\text{opt}}$ , we may need to compute a large amount of log-likelihoods for different networks  $\mathcal{G}$ , hence the efficiency of the forward solver is crucial to make the optimisation procedure feasible. This rules out a possibility of solving (2) directly due to the curse of dimensionality.

## 2.3 Stochastic simulation algorithms for forward problem

Traditionally, probabilities  $p(\mathbf{x}, t)$  are estimated using the Stochastic Simulation Algorithm (SSA) [29], or some more efficient (e.g. multilevel) Monte Carlo simulations of the realisations of the model [30, 39, 3, 51]. Essentially, these methods sample  $N_{\text{SSA}}$  random walks

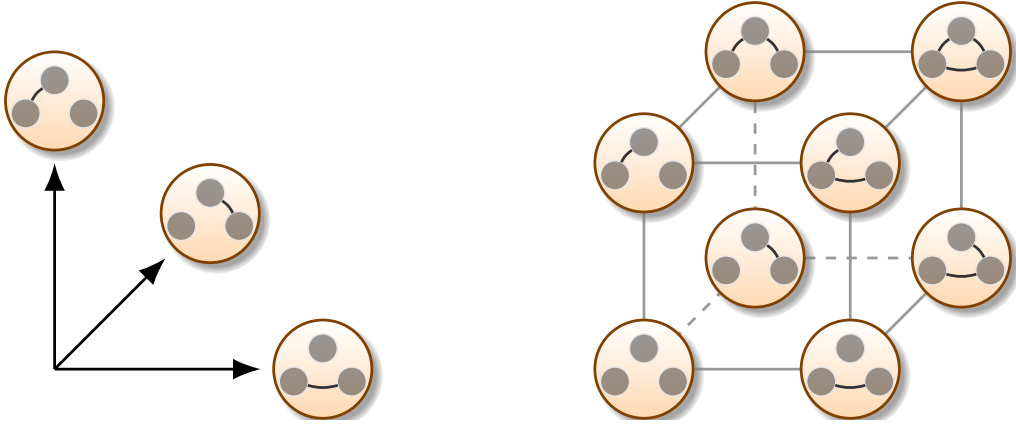


Figure 3: The set of all possible networks with  $N = 3$  nodes is a binary hypercube in dimension  $\frac{1}{2}N(N - 1) = 3$ .

through the state space  $\Omega$  starting at the initial state  $x_{k-1}$ , count the number  $n_{\text{SSA}}$  of trajectories that end up in the state  $x_k$  by the time  $t_k$ , and estimate the target probability as a frequency,

$$P(x_{k-1} \rightarrow x_k | \mathcal{G}) \approx \tilde{P}(x_{k-1} \rightarrow x_k | \mathcal{G}) = \frac{n_{\text{SSA}}}{N_{\text{SSA}}}. \quad (5)$$

The cost of sampling each trajectory does not grow exponentially with  $N$  which makes these methods free from the curse of dimensionality. However, the convergence of these algorithms is not particularly fast, with typical estimates

$$\text{err} = \left| P(x_{k-1} \rightarrow x_k | \mathcal{G}) - \tilde{P}(x_{k-1} \rightarrow x_k | \mathcal{G}) \right| \leq c N_{\text{SSA}}^{-\delta},$$

with  $0.5 \leq \delta \leq 1$  depending on a particular method. This is usually sufficient to estimate large probabilities and main statistics (such as mean and variance) of the process. However, if the probability  $p = P(x_{k-1} \rightarrow x_k | \mathcal{G})$  is small, to ensure the desired relative precision  $|p - \tilde{p}| \leq \epsilon p$ , the number of samples should satisfy  $c N_{\text{SSA}}^{-\delta} \leq \epsilon p$ , or  $N_{\text{SSA}} \geq (\epsilon p / c)^{-1/\delta}$ . In practice this means that estimation of rare events with probabilities  $p \lesssim 10^{-6}$  with these algorithms can be prohibitively expensive.

If the computational budget of  $N_{\text{SSA}}$  trajectories is exhausted and none of them arrived at  $x_k$ , then  $n_{\text{SSA}} = 0$  and  $\tilde{p} = 0$ , i.e. the event is not resolved with the algorithm and is considered impossible. If this happens for at least one transition from state  $x_{k-1}$  to  $x_k$  for some  $k = 1, \dots, K$ , then the whole likelihood  $L(\mathcal{G}) = 0$  for the given network  $\mathcal{G}$ . In practical computations this issue can occur for most networks  $\mathcal{G} \neq \mathcal{G}_*$  except the ‘ground truth’ network and its close neighbours. The limited computation budget for the forward problem therefore leads to flattening of the high-dimensional landscape of the likelihoods, wiping off the structural information that should be used to navigate the optimisation algorithm towards the solution of (4). This motivates the development of more accurate methods for the forward problem, such as the tensor product approach that we discuss in the following subsection.

## 2.4 Tensor product algorithms for forward problem

To find the probabilities composing the likelihood (4), we can solve the system of ODEs (2) for the probabilities of the network states. This system is commonly known as the chemical master equation (CME) and consists of  $|\Omega| = 2^N$  equations and unknowns, hence traditional solvers suffer from the curse of dimensionality. To mitigate this problem, different approaches were used, including sparse grids [37], adaptive finite state projections [58, 43, 11],

radial basis functions [50], neural networks [34, 69], and tensor product approximations, such as canonical polyadic (CP) format [44, 2, 38], and more recently tensor train (TT) format [45, 19, 23, 22, 73, 18, 42, 28, 21]. Here we briefly describe the tensor train approach used in our recent paper [21].

First, we note that among  $2^N$  reaction rates  $p_{y \rightarrow x}$  in (2) only  $2N$  are non-zero, according to (1):

$$p'(x, t) = \sum_{n=1}^N \left( p_{(x-e_n) \rightarrow x}^{(\text{inf})} p(x - e_n, t) + p_{(x+e_n) \rightarrow x}^{(\text{rec})} p(x + e_n, t) - \left( p_{x \rightarrow (x+e_n)}^{(\text{inf})} + p_{x \rightarrow (x-e_n)}^{(\text{rec})} \right) p(x, t) \right), \quad (6)$$

for  $x \in \Omega$ . Let us now uncover the tensor product structure of the matrix of this CME, assuming that the probability  $p(x, t)$  of the network state  $x = (x_1, \dots, x_N)^T$  appears in the probability distribution function (p.d.f.) vector  $\mathbf{p}(t) = [p(x, t)]_{x \in \Omega}$  in position  $\overline{x_1 x_2 \dots x_N} = 2^{N-1}(x_1 - 1) + 2^{N-2}(x_2 - 1) + \dots + 2^0 x_N$ .

Using *indicator* function

$$\mathbf{1}_{\text{condition}} = \begin{cases} 1, & \text{if condition is true} \\ 0, & \text{if condition is false,} \end{cases}$$

we can write  $p_{x \rightarrow (x-e_n)}^{(\text{rec})} = \gamma \mathbf{1}_{x_n=1}$ , and  $p_{x \rightarrow (x+e_n)}^{(\text{inf})} = (\varepsilon + \beta \sum_{m \sim n} \mathbf{1}_{x_m=1}) \mathbf{1}_{x_n=0}$ . Collecting these reaction rates in vectors of size  $2^N$ , and using the *big-endian* ordering as explained above, we obtain tensor product decompositions

$$\left[ p_{x \rightarrow (x-e_n)}^{(\text{rec})} \right]_{x \in \Omega} = \gamma \vec{e} \otimes \dots \otimes \vec{e} \otimes \vec{i} \otimes \vec{e} \otimes \dots \otimes \vec{e}, \quad (7)$$

where  $\vec{i} = (0 \ 1)^T$  appears in position  $n$ ,  $\vec{e} = (1 \ 1)^T$  appear elsewhere; and

$$\begin{aligned} \left[ p_{x \rightarrow (x+e_n)}^{(\text{inf})} \right]_{x \in \Omega} &= \varepsilon \vec{e} \otimes \dots \otimes \vec{e} \otimes \vec{s} \otimes \vec{e} \otimes \dots \otimes \vec{e} \\ &+ \beta \sum_{m \sim n} \vec{e} \otimes \dots \otimes \vec{e} \otimes \vec{s} \otimes \vec{e} \otimes \dots \otimes \vec{e} \otimes \vec{i} \otimes \vec{e} \otimes \dots \otimes \vec{e}, \end{aligned} \quad (8)$$

where  $\vec{s} = (1 \ 0)^T$  appears in position  $n$ ,  $\vec{i} = (0 \ 1)^T$  appear in positions  $m \sim n$ ,  $\vec{e} = (1 \ 1)^T$  appear elsewhere. To complete the expansion for the right-hand side of (6), we need to express the shifted state  $p(x - e_n, t)$  as a sum over probabilities  $p(y, t)$  as follows

$$\begin{aligned} p(x - e_n, t) &= \sum_{y \in \Omega} \mathbf{1}_{x_1=y_1} \dots \mathbf{1}_{x_{n-1}=y_{n-1}} \cdot \mathbf{1}_{x_n-1=y_n} \cdot \mathbf{1}_{x_{n+1}=y_{n+1}} \dots \mathbf{1}_{x_N=y_N} \cdot p(y, t), \\ \left[ p(x - e_n, t) \right]_{x \in \Omega} &= \underbrace{(\text{Id} \otimes \dots \otimes \text{Id} \otimes J^T \otimes \text{Id} \otimes \dots \otimes \text{Id})}_{\mathbf{J}_n^T} \mathbf{p}(t), \end{aligned} \quad (9)$$

where the *shift matrix*  $J^T = \begin{pmatrix} 0 & 0 \\ 1 & 0 \end{pmatrix}$  appears in position  $n$ , and identity matrices  $\text{Id} = \begin{pmatrix} 1 & 0 \\ 0 & 1 \end{pmatrix}$  appear elsewhere. Similarly,  $\left[ p(x + e_n, t) \right]_{x \in \Omega} = \mathbf{J}_n \mathbf{p}$  with  $\mathbf{J}_n = \text{Id} \otimes \dots \otimes \text{Id} \otimes J \otimes \text{Id} \otimes \dots \otimes \text{Id}$ . Combining the above, we collect all equations of (6) in a vectorised CME

$$\mathbf{p}'(t) = \mathbf{A} \mathbf{p}(t), \quad \mathbf{p}(0) = \mathbf{p}_0, \quad (10)$$



where the  $2^N \times 2^N$  matrix  $\mathbf{A}$  admits the following tensor product form:

$$\begin{aligned} \mathbf{A} = & \gamma \sum_{n=1}^N \text{Id} \otimes \cdots \otimes \text{Id} \otimes (J - \text{Id}) \text{diag}(\vec{\tau}) \otimes \text{Id} \otimes \cdots \otimes \text{Id} \\ & + \varepsilon \sum_{n=1}^N \text{Id} \otimes \cdots \otimes \text{Id} \otimes (J^T - \text{Id}) \text{diag}(\vec{s}) \otimes \text{Id} \otimes \cdots \otimes \text{Id} \\ & + \beta \sum_{n=1}^N \sum_{m \sim n} \text{Id} \otimes \cdots \otimes \text{Id} \otimes (J^T - \text{Id}) \text{diag}(\vec{s}) \otimes \text{Id} \otimes \cdots \otimes \text{Id} \otimes \text{diag}(\vec{\tau}) \otimes \text{Id} \otimes \cdots \otimes \text{Id}. \end{aligned} \quad (11)$$

This so-called canonical polyadic (CP) [41, 36, 12] form represents the CME matrix  $\mathbf{A}$  as a sum of  $(2N + |\mathcal{E}|)$  elementary tensors, each of which is a direct product of  $N$  small  $2 \times 2$  matrices, acting on a single node of the network only. Hence, the storage for  $A$  reduces from  $\mathcal{O}(2^N \langle k \rangle)$  down to  $\mathcal{O}((2N + \langle k \rangle)N)$  elements, where  $\langle k \rangle = |\mathcal{E}|/|\mathcal{V}|$  denotes the average degree of  $\mathcal{G}$ . The curse of dimensionality for the matrix is therefore removed.

To remove the exponential complexity in solving (10), we need to achieve a similar compression for the p.d.f.  $\mathbf{p}(t) = [p(x, t)]_{x \in \Omega}$ , for which we employ the *tensor train* (TT) format [60].

$$\mathbf{p} \approx \tilde{\mathbf{p}} = \sum_{\alpha_0, \dots, \alpha_N=1}^{r_0, \dots, r_N} \mathbf{p}_{\alpha_0, \alpha_1}^{(1)} \otimes \cdots \otimes \mathbf{p}_{\alpha_{n-1}, \alpha_n}^{(n)} \otimes \cdots \otimes \mathbf{p}_{\alpha_{N-1}, \alpha_N}^{(N)}. \quad (12)$$

Here, the  $r_{n-1} \times 2 \times r_n$  factors  $\mathbf{p}^{(n)} = [\mathbf{p}_{\alpha_{n-1}, \alpha_n}^{(n)}(x_n)]$ ,  $n = 1, \dots, N$ , are called *TT cores*, and the ranges of the summation indices  $r_0, \dots, r_N$  are called *TT ranks*. Each core  $\mathbf{p}^{(n)}$  contains information related to node  $n$  in the network, and the summation indices  $\alpha_{n-1}, \alpha_n$  of core  $\mathbf{p}^{(n)}$  link it to cores  $\mathbf{p}^{(n-1)}$  and  $\mathbf{p}^{(n+1)}$ . The matrix–vector multiplication can be performed fully in tensor product format. Using recently proposed algorithms [23, 22] the linear system of ODEs (10) can be solved fully in the TT format avoiding the curse of dimensionality, as explained in details in [21].

## 2.5 Ordering of network nodes for faster forward problem solving

The TT decomposition of probability functions exhibits low ranks when distant (with respect to their position in the state vector) variables are weakly correlated; see e.g. [65] for a rigorous analysis of this for the multivariate normal probability density function. Numerical approaches to order the variables in such a way include a greedy complexity optimisation over a reduced space of permutations [4, 55], using gradients to compute a Fisher–type information matrix and its eigenvalue decomposition to sort or rotate the variables [15], and sorting the variables according to the Fiedler vector of the network [5]. Since in our case the variables are discrete, we adopt the latter approach.

We consider the Laplacian matrix of the network  $\mathcal{G}$ , defined as follows

$$L = \text{diag}(Ge) - G, \quad (13)$$

where  $G \in \mathbb{B}^{N \times N}$  is the adjacency matrix of  $\mathcal{G}$ , and  $\mathbf{e} = (1 \ 1 \ \cdots \ 1)^T \in \mathbb{B}^N$ . We are particularly interested in the *Laplacian spectrum* of  $\mathcal{G}$ , i.e. solutions to the eigenvalue problem  $Lu = \lambda u$ . It is easy to see that since  $G = G^T$  we also have  $L = L^T$ , hence the spectrum is real,  $\lambda \in \mathbb{R}$ . We also note that  $L = [\ell_{m,n}]_{m,n \in \mathcal{V}}$  is diagonally dominant, since  $\ell_{m,m} = \sum_{n \in \mathcal{V}} g_{m,n} \geq 0$ , and  $\ell_{m,n} = -g_{m,n} \leq 0$  for  $m \neq n$ , hence  $|\ell_{m,m}| = \sum_{m \neq n} |\ell_{m,n}|$ . Since  $\text{diag}(L) \geq 0$  and  $L$  is

symmetric and diagonally dominant, the Laplacian is positive semi-definite, hence its eigenvalues are nonnegative,  $\lambda_{n-1} \geq \lambda_{n-2} \geq \dots \geq \lambda_1 \geq \lambda_0 \geq 0$ . It is easy to see that  $Le = 0$ , hence  $\lambda_0 = 0$  is the lowest eigenvalue with the corresponding eigenvector  $u_0 = e$ .

The second eigenvalue, which we denote  $\lambda_1$ , is called the *algebraic connectivity* of  $\mathcal{G}$  or *Fiedler value*. It was known since [26] that  $\lambda_1 = 0$  if and only if  $\mathcal{G}$  is disconnected. This is a particularly easy scenario for epidemiological modelling. If  $\mathcal{G}$  consists of two disjoint networks,  $\mathcal{G}_1$  and  $\mathcal{G}_2$ , then nodes from  $\mathcal{G}_1$  and  $\mathcal{G}_2$  can not affect each other. The random variables associated with those nodes are therefore independent, i.e. if  $X_1 \in \mathcal{G}_1$  and  $X_2 \in \mathcal{G}_2$  then  $P(X_1, X_2) = P(X_1)P(X_2)$ . This means that if we order the variables  $x_1, \dots, x_N$  in such a way that the first block  $x_1, \dots, x_m \in \mathcal{G}_1$  and the second block  $x_{m+1}, \dots, x_N \in \mathcal{G}_2$  do not overlap, then the TT format (12) for the p.d.f.  $p(x_1, \dots, x_N)$  will have the TT rank  $r_m = 1$  for the connection separating  $\mathcal{G}_1$  and  $\mathcal{G}_2$ .

These geometric properties of the network can be estimated from the eigenvector  $v = u_1$ , also known as *Fiedler vector*. In the pioneering paper [27] it was related to finding an optimal cut in the network  $\mathcal{G}$ . It was generalised to reducing the envelope (or the bandwidth) of the adjacency matrix  $G$  in [6], and later to finding orderings of variables for which TT decomposition (12), and related MPS and DMRG representations in quantum physics [66], have lower TT ranks [5]. The Fiedler vector can be computed by minimising the *Rayleigh quotient*  $v = \arg \min_{v \perp e} v^T L v / \|v\|^2$ , also known as the *Courant minimax* principle, orthogonally to  $u_0 = e$ . Following [6], we use the Fiedler vector to define a one-dimensional embedding of the graph to a linear chain. Let  $\sigma \in \mathfrak{S}_n$  be the permutation vector of the set of nodes  $\mathcal{V}$  such that  $(v_{\sigma})$  is ordered, i.e.  $v_{\sigma_1} \geq v_{\sigma_2} \geq \dots \geq v_{\sigma_N}$ , or equivalently in the ascending order. Following [5], the same permutation of variables also reduces the TT ranks of the TT decomposition (12). In particular, it groups together variables corresponding to independent subgrids. Hence, we compute this permutation and adopt its order of variables before solving the forward problem (10) using tensor product algorithms.

## 2.6 Algorithms for Bayesian inverse problem

Since the full grid search is unfeasible for even moderate networks, we adopt the Metropolis–Hastings Markov Chain Monte Carlo (MCMC) method to approach the maximum of  $L(\mathcal{G})$ . The method is depicted in Algorithm 1. We need to choose a *proposal distribution*  $q(\hat{\mathcal{G}}|\mathcal{G})$  which is tractable for sampling a new state of the network  $\hat{\mathcal{G}}$ , given the current network  $\mathcal{G}$ . In each iteration, given the current network  $\mathcal{G}_i$ , we sample a new proposal  $\hat{\mathcal{G}}$  and accept or reject it probabilistically based on the Metropolis–Hastings ratio, forming a Markov Chain of network configurations  $\mathcal{G}_0, \mathcal{G}_1, \dots$ . After the Markov Chain is computed, we return the sample of this chain with the maximal likelihood. This algorithm is known to converge to the true distribution  $\frac{1}{Z}L(\mathcal{G})$  (where  $Z$  is the normalising constant) under mild assumptions [64]. In practice, we use two proposal distributions.

1. Choose one link in  $\mathcal{G}_i$  uniformly at random and toggle its state (on/off). Since there are  $N(N-1)/2$  possible links to toggle,  $q(\hat{\mathcal{G}}|\mathcal{G}) = \frac{2}{N(N-1)}$  independently of  $\hat{\mathcal{G}}$  and  $\mathcal{G}$ , and hence cancels in the Metropolis-Hastings ratio. We will call Algorithm 1 with this proposal “MCMC”.
2. Every  $N(N-1)/2$  iterations (i.e. when  $\text{mod}(n, N(N-1)/2) = 0$ ), sample a random permutation vector  $\sigma \in \mathfrak{S}_{N(N-1)/2}$  of the set  $\{1, \dots, N(N-1)/2\}$ , and in the next  $N(N-1)/2$  iterations toggle links in the order prescribed by  $\sigma$ . This is still a valid MCMC algorithm with a constant proposal distribution, but now with respect to  $\sigma$ , corresponding to a collection of networks in consecutive update steps,  $(\mathcal{G}_{i+1}, \dots, \mathcal{G}_{i+N(N-1)/2})$ . However, as we will observe in the numerical experiments, this algorithm can often increase

---

**Algorithm 1** MCMC algorithm for the likelihood maximization
 

---

- 1: Choose the proposal distribution  $q(\hat{\mathcal{G}}|\mathcal{G})$ , initial network  $\mathcal{G}_0$  and length of the chain  $N_{\text{eval}}$ .
  - 2: **for**  $i = 0, \dots, N_{\text{eval}} - 1$  **do**
  - 3:   Sample a new proposal network  $\hat{\mathcal{G}} \sim q(\hat{\mathcal{G}}|\mathcal{G}_i)$ .
  - 4:   Compute the Metropolis–Hastings ratio  $h(\hat{\mathcal{G}}, \mathcal{G}_i) = \frac{L(\hat{\mathcal{G}}) q(\mathcal{G}_i|\hat{\mathcal{G}})}{L(\mathcal{G}_i) q(\hat{\mathcal{G}}|\mathcal{G}_i)}$ .   ▷ As shown in (14).
  - 5:   Sample a uniformly distributed random number  $r \sim \mathcal{U}(0, 1)$ .
  - 6:   **if**  $r < \min(h(\hat{\mathcal{G}}, \mathcal{G}_i), 1)$  **then**
  - 7:     Accept the proposal by setting  $\mathcal{G}_{i+1} = \hat{\mathcal{G}}$ .
  - 8:   **else**
  - 9:     Reject the proposal by setting  $\mathcal{G}_{i+1} = \mathcal{G}_i$ .
  - 10:   **end if**
  - 11: **end for**
  - 12: **return**  $\mathcal{G}_* = \arg \max_{i=0, \dots, N_{\text{eval}}} \log L(\mathcal{G}_i)$ .
- 

the likelihood faster in terms of the individual link changes, and hence the computing time. In each block of  $N(N-1)/2$  iterations, this algorithm proposes link changes without replacement [67]. For this reason, we will call this algorithm “MCMC noR” (for “no Replacement”).

Cancelling the constant proposal probability, and using log-likelihoods to avoid numerical over- and under-flow errors, we arrive at the following formula for the Metropolis–Hastings ratio:

$$h(\hat{\mathcal{G}}, \mathcal{G}_i) = \exp \left( \log L(\hat{\mathcal{G}}) - \log L(\mathcal{G}_i) \right). \quad (14)$$

## 2.7 Choosing initial guess for optimisation

A good initial guess  $\mathcal{G}_0$  for the contact network can significantly improve the computational efficiency by reducing the number of steps required by the optimisation algorithm to converge towards the optimum  $\mathcal{G}_{\text{opt}}$ , but also by simplifying the forward problems and hence reducing the computational time required to evaluate each likelihood  $L(\mathcal{G})$  in (4). Here we present a simple algorithm to generate an initial guess using the given nodal time series data  $\mathcal{X} = \{t_k, \mathbf{x}_k\}_{k=0}^K$ . By comparing each next state  $\mathbf{x}_k$  against a previous one  $\mathbf{x}_{k-1}$  for  $k = 1, \dots, K$  node-by-node, we observe events of two possible types: infected nodes that become susceptible (recovery), and susceptible nodes becoming infected (infection). Recoveries are single-node events and provide no information on the network connectivity. In contrast, infections are two-node events that occur when a susceptible node is connected to an infected node. Therefore, any node  $m$  that was or became infected during  $t \in [t_{k-1}, t_k]$  could have infected any connected susceptible node  $n$  that became infected during the same time interval.

Thus, we compute the connectivity scores  $h_{m,n}$  for all  $m, n \in \mathcal{V}$  as follows

$$h_{m,n} = \sum_{k=1}^K h_{m,n}^{(k)}, \quad \text{with} \quad h_{m,n}^{(k)} = \begin{cases} \frac{1}{|\mathcal{I}_k|}, & \text{if } x_{n,k-1} = 0, x_{n,k} = 1, \text{ and } m \in \mathcal{I}_k; \\ 0, & \text{otherwise,} \end{cases} \quad (15)$$

where  $\mathcal{I}_k = \{m \in \mathcal{V} : x_{m,k-1} = 1 \text{ or } x_{m,k} = 1\}$  is the set of all infected nodes at the beginning or by the end of the interval  $t \in [t_{k-1}, t_k]$ . The higher is the acquired score  $h_{m,n}$  the higher is the evidence that  $m \sim n$  in the contact network. Hence, when the scores are calculated, we can sample an initial guess network  $\mathcal{G}_0$  randomly with probabilities for each link proportional to the scores. Alternatively, for a more deterministic approach, we can discretise the distribution, and set  $m \sim n$  in  $\mathcal{G}_0$  for all links  $(m, n)$  for which the score exceeds the average,  $h_{m,n} \geq \frac{2}{N(N-1)} \sum_{i>j} h_{i,j}$ .

### 3 Results

The numerical experiments were implemented in Matlab 2022b based on TT-Toolbox<sup>1</sup> and tAMEn<sup>2</sup> packages, and run on one node of the HC44 series of the University of Bath “Nimbus” Microsoft Azure cluster, parallelising experiments with different datasets over 42 cores of the Intel Xeon Platinum 8168 CPUs. Each of these parallel processes ran in a single-threaded mode.

The codes are publicly available from [github.com/savostyanov/ttsir](https://github.com/savostyanov/ttsir).

#### 3.1 Linear chain

For this experiment we generated  $N_s = 42$  samples of synthetic data by computing random walks of  $\varepsilon$ -SIS process with parameters  $\beta = 1$ ,  $\gamma = 0.5$  and  $\varepsilon = 0.01$  for the duration of  $T = 200$  time units. The trajectories were then re-sampled to a uniform grid on  $[0, T]$  with the time step  $\tau = 0.1$  to imitate data collected at regular intervals. Therefore, each trajectory contained  $K = 2000$  data records representing the epidemic process. Data were created using the ‘ground truth’ network  $\mathcal{G}_*$  which is a linear chain with  $N = 9$  nodes as shown in Fig. 4(a), and assuming that the initial state  $\mathbf{x}_0 = (1, 0, \dots, 0)$  is the same for all data samples.

First, we checked the contrast of the log-likelihood at the ground truth network  $\mathcal{G}_*$ , by computing  $E[\log_{10} L(\mathcal{G}) - \log_{10} L(\mathcal{G}_*)]$  averaged over the  $N_s = 42$  sampled datasets. We calculate this value for all  $\mathcal{G}$  that are nearest neighbours of  $\mathcal{G}_*$ , i.e. differ by only one link. The results are shown on Fig. 4(b). We note that removal of an existing link from  $\mathcal{G}_*$  results in a contrast  $E[\log_{10} L(\mathcal{G}) - \log_{10} L(\mathcal{G}_*)] \simeq -50$ , raising to  $\simeq -60$  for links attached to the sides of the chain. This is easy to understand, as removal of a link from  $\mathcal{G}_*$  creates a disconnected graph  $\mathcal{G}$ , where two subgraphs can not pass the infection on to each other, hence the epidemic dynamics on  $\mathcal{G}$  differs significantly from the one on  $\mathcal{G}_*$ . Adding a new link to  $\mathcal{G}_*$  results in a milder contrast  $E[\log_{10} L(\mathcal{G}) - \log_{10} L(\mathcal{G}_*)] \in [-30, -10]$ , because the grid remains connected and the dynamics of the epidemic is less affected. This confirms that  $\mathcal{G}_*$  is at least a local optimum for  $\log L(\mathcal{G})$ , and therefore can be inferred by Bayesian optimisation, assuming the optimisation algorithm manages to converge to it.

Secondly, we evaluated probabilities  $P(\mathbf{x}_{k-1}^{(n_s)} \rightarrow \mathbf{x}_k^{(n_s)} | \mathcal{G})$  in (4) for all data records  $k = 1, \dots, K$  for all generated datasets  $n_s = 1, \dots, N_s$ . The results are shown in Fig. 4(c) for the initial guess network  $\mathcal{G} = \mathcal{G}_0$  computed as explained in Sec. 2.7, and in Fig. 4(d) for the ground truth network  $\mathcal{G} = \mathcal{G}_*$ . We used the SSA algorithm [29] with  $N_{\text{SSA}} = 10^3$  samples as explained in Sec. 2.3. A significant number of events are not resolved by SSA and the probabilities are estimated as zero, as shown by the  $\log_{10} p = -\infty$  column on the histograms. We then computed the same probabilities by solving the CME (10) subject to initial condition  $\mathbf{x}_{k-1}^{(n_s)}$  on time interval  $t \in [t_{k-1}, t_k]$ , for which we apply the tAMEn algorithm [22] with Chebyshev polynomials of degree 12 in time and relative accuracy threshold  $\epsilon_{\text{tAMEn}} = 10^{-6}$ . From the tAMEn algorithm we obtain the whole p.d.f.  $\mathbf{p}(t) = [p(\mathbf{x}, t)]_{\mathbf{x} \in \Omega}$  for  $t \in [t_{k-1}, t_k]$  and for all states  $\mathbf{x} \in \Omega$ , from which we extract the required probability by projecting to the deterministic final state  $\mathbf{x}_k^{(n_s)}$ .

We observe that 1.7% of probabilities are unresolved by SSA for  $\mathcal{G} = \mathcal{G}_0$  and 1.1% of probabilities are unresolved for  $\mathcal{G} = \mathcal{G}_*$ , which is nevertheless sufficient for both likelihoods  $L(\mathcal{G}_0) = 0$  and  $L(\mathcal{G}_*) = 0$  to be unresolved for 100% of data samples  $n_s = 1, \dots, N_s$ .

The number of SSA trajectories is set to approximately match the computational time of SSA and tensor product algorithms for the forward problem. With tAMEn, the trajectories  $\mathbf{p}(t)$  are computed in the TT format (12) for which the TT ranks are determined adaptively.

<sup>1</sup><https://github.com/oseledets/TT-Toolbox>

<sup>2</sup><https://github.com/dolgov/tamen>

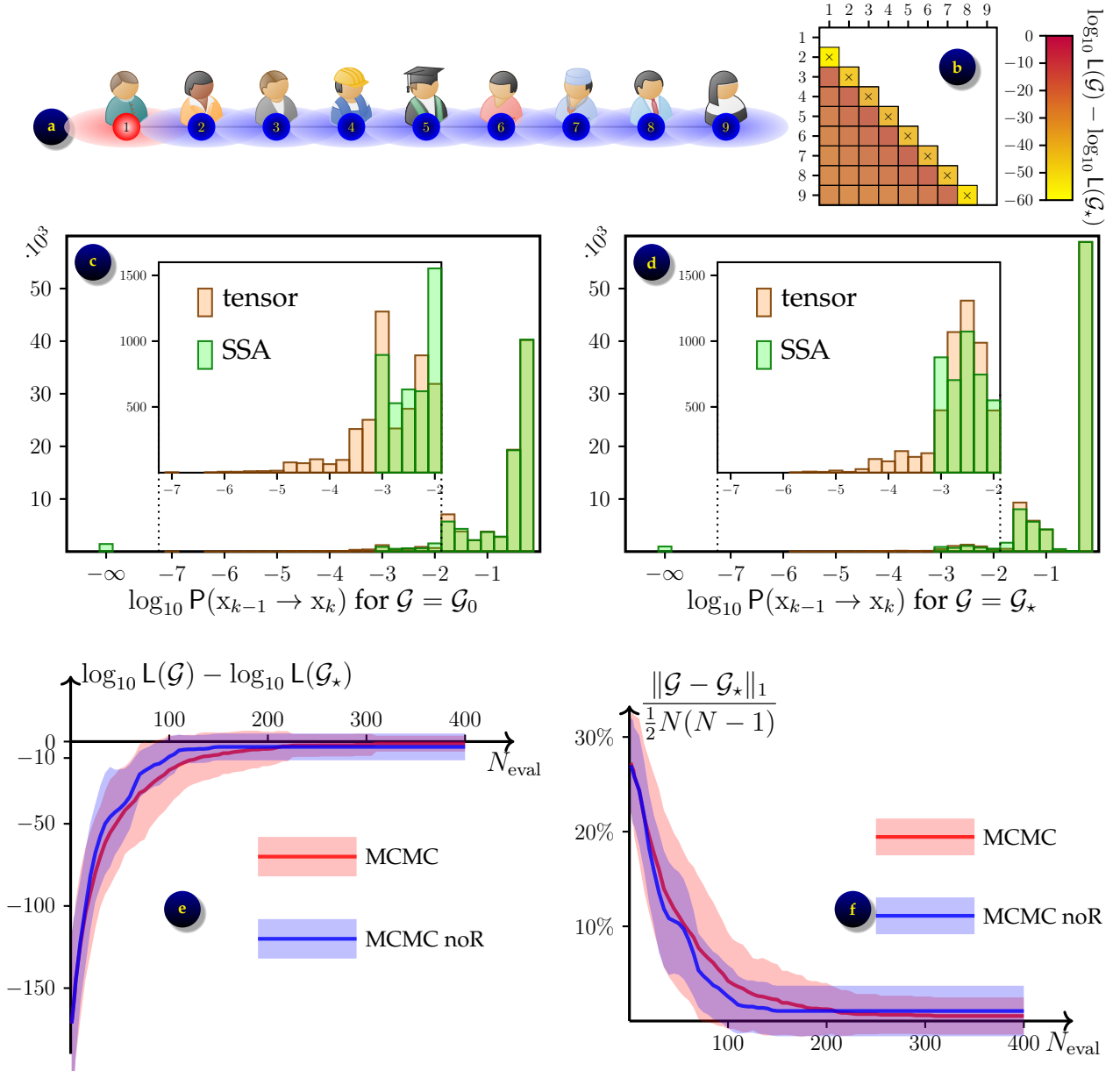


Figure 4: Inferring linear chain network with  $N = 9$  people from  $\varepsilon$ -SIS epidemic process with  $\beta = 1$ ,  $\gamma = 0.5$  and  $\varepsilon = 0.01$ : (a) the network  $\mathcal{G}_*$  in its initial state; (b) the contrast  $\log_{10} L(\mathcal{G}) - \log_{10} L(\mathcal{G}_*)$  averaged over  $N_s = 42$  datasets, shown for grids  $\mathcal{G}$  that differ from  $\mathcal{G}_*$  by a single link  $(m, n)$ ; axes  $\times$  show connected nodes in  $\mathcal{G}_*$ ; (c) the distribution of probabilities for the transitions observed in data for the initial guess network  $\mathcal{G}_0$ ; (d) the distribution of probabilities for the transitions observed in data for the ground truth network  $\mathcal{G}_*$ ; (e) convergence of likelihood  $L(\mathcal{G})$  towards  $L(\mathcal{G}_*)$  in the optimisation process; average (solid lines)  $\pm$  one standard deviation (shaded areas) over the  $N_s = 42$  datasets; (f) convergence of network  $\mathcal{G}$  towards  $\mathcal{G}_*$ .

For this example we observe TT ranks  $r \simeq 14.8 \pm 2.3$  for  $\mathcal{G} = \mathcal{G}_0$  and  $r \simeq 11.1 \pm 0.9$  for  $\mathcal{G} = \mathcal{G}_*$  leading to computational time for the likelihood  $L(\mathcal{G})$  to be CPU time  $\simeq 98 \pm 6.9$  seconds for  $\mathcal{G} = \mathcal{G}_0$  and CPU time  $\simeq 80 \pm 3.2$  seconds for  $\mathcal{G} = \mathcal{G}_*$ . With the SSA algorithm, one likelihood computation took CPU time  $\simeq 199 \pm 23.5$  seconds for  $\mathcal{G} = \mathcal{G}_0$  and CPU time  $\simeq 107 \pm 6.3$  seconds for  $\mathcal{G} = \mathcal{G}_*$ . Note that the forward problems become easier to solve as the optimisation process approaches the ground truth network both because the linear geometry of the chain matches the structure of the TT format, and because the easier reaction network admits larger time steps in SSA. Due to the simplicity of the linear structure, a linear chain is an attractive model for study in quantum physics, see e.g a recent paper on the SIS model on a linear chain [54].

We performed the black-box Bayesian optimisation using  $N_{\text{eval}} = 400$  steps of the MCMC algorithms with and without replacement as explained in Sec. 2.6. The results are shown in Fig. 4(d) for the convergence of the likelihood  $L(\mathcal{G})$  towards the one of the ground truth network,  $L(\mathcal{G}_*)$ , and in Fig. 4(e) for the corresponding convergence of the network  $\mathcal{G}$  towards the ground truth network  $\mathcal{G}_*$ . The latter is measured using the number of incorrectly inferred links,

$$\|\mathcal{G} - \mathcal{G}_*\|_1 = |\{m, n \in \mathcal{V}, m > n : g_{m,n} \neq g_{m,n}^*\}|, \quad (16)$$

related to the total number of possible links,  $\frac{1}{2}N(N-1)$ . With both algorithms we observe a steady convergence towards optimum with the ground truth grid correctly inferred in 40 out of 42 experiments and one link inferred incorrectly in 2 out of 42 experiments after  $N_{\text{eval}} = 400$  likelihood evaluations. In total for this experiment, the network inference from each dataset with  $K = 2000$  records took about  $33 \cdot 10^3$  seconds.

### 3.2 Austria road network

For this experiment we considered a more realistic example of a contact network, drawn from the road network in Austria, shown in Fig. 5(a). From preliminary experiments we noted that both MCMC algorithms for Bayesian optimisation struggle to converge to the optimum. To partly mitigate this, we increased the size of the dataset. We generated  $N_s = 42$  samples of synthetic data for a  $\varepsilon$ -SIS model with per contact transfer rate  $\beta = 1$ , individual recovery rate  $\gamma = 0.5$  and self-infection rate  $\varepsilon = 0.01$ , for the duration of  $T = 1000$  time units, and again re-sampled the data to a uniform grid with the time step  $\tau = 0.1$ , hence creating  $K = 10^4$  data records for each data sample.

From the contrasts shown on Fig. 5(b), we see that removal of any of two links that produces a disconnected graph  $\mathcal{G}$  results in a very high contrast,  $E[\log_{10} L(\mathcal{G}) - \log_{10} L(\mathcal{G}_*)] \lesssim -400$ . Removing or adding other links results in a connected  $\mathcal{G}$  and hence a moderate value of the contrast  $E[\log_{10} L(\mathcal{G}) - \log_{10} L(\mathcal{G}_*)] \in [-100, -15]$ .

Similarly to the previous example, we observe that SSA with  $n_{\text{SSA}} = 10^3$  samples does not resolve a significant number of events along the trajectory, and therefore returns  $\tilde{P}(x_{k-1} \rightarrow x_k | \mathcal{G}) = 0$  for 5.6% of data points for the initial guess network  $\mathcal{G} = \mathcal{G}_0$  and for 2.0% of data points for the ground truth network  $\mathcal{G} = \mathcal{G}_*$ , leading to the likelihood  $L(\mathcal{G}) = 0$  being unresolved in all experiments for both grids. Note that the proportion of unresolved (rare) events is larger for this example due to a more complex network structure.

Using the tensor product approach with the same parameters as in Sec. 3.1 for the forward problem, we were able to resolve probabilities of up to  $p \sim 10^{-7}$ , which produced non-zero values for all likelihoods  $L(\mathcal{G})$ , enabling the optimisation for the inverse problem. For this example, one likelihood evaluation solving the forward problem with tAMEn took CPU time  $\simeq 431 \pm 8.2$  seconds for  $\mathcal{G} = \mathcal{G}_0$  and CPU time  $\simeq 439 \pm 4.8$  seconds for  $\mathcal{G} = \mathcal{G}_*$ . The main reason for the larger times compared to the previous experiment is the larger data size  $K = 10^4$  compared to  $K = 2000$  for the linear chain. However, a more complex structure

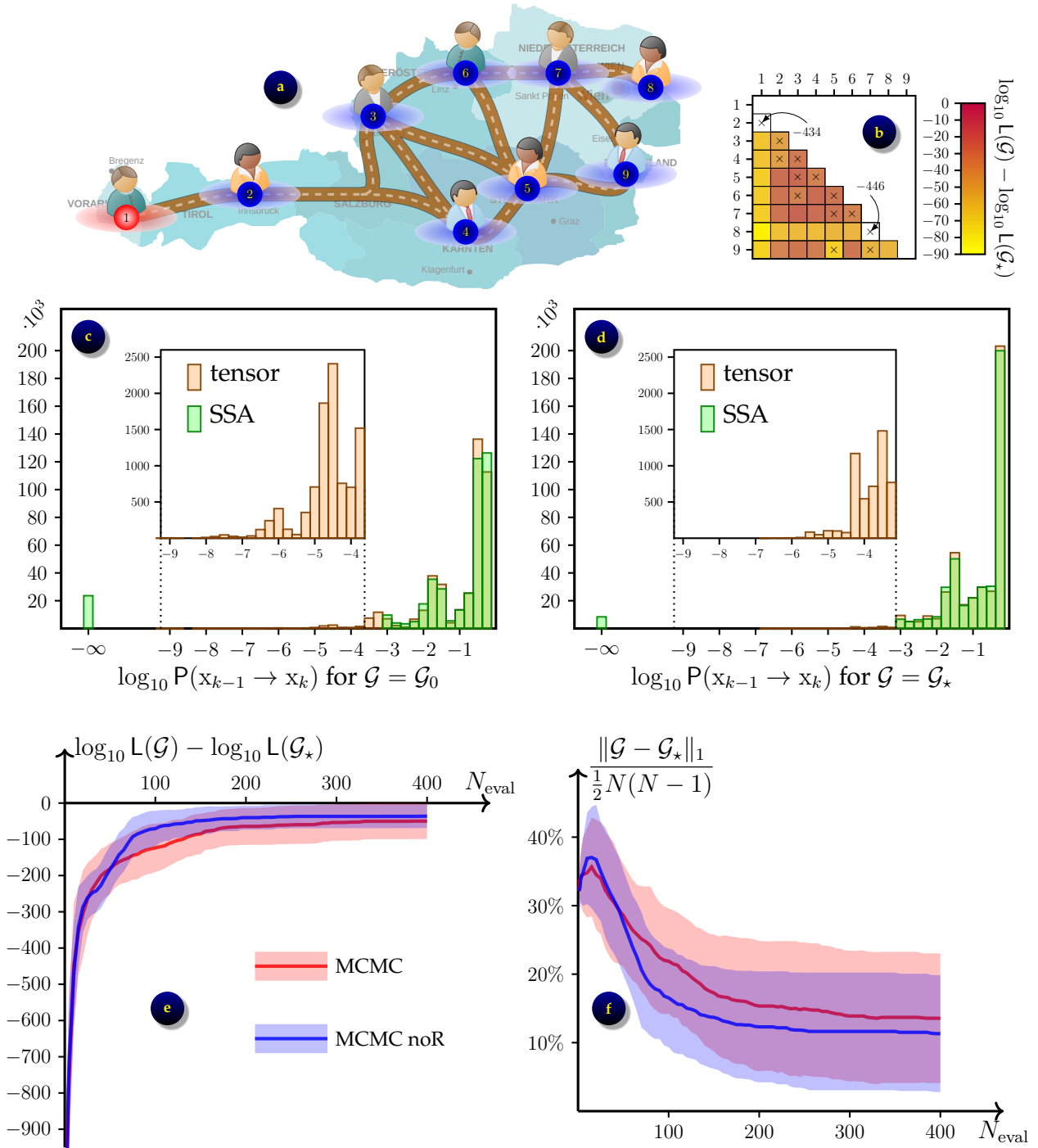


Figure 5: Inferring a road network in Austria ( $N = 9$  nodes) from  $\varepsilon$ -SIS epidemic process with  $\beta = 1$ ,  $\gamma = 0.5$  and  $\varepsilon = 0.01$ : (a) the network  $\mathcal{G}_*$  in its initial state; (b) the contrast  $\log_{10} L(\mathcal{G}) - \log_{10} L(\mathcal{G}_*)$  averaged over  $N_s = 42$  datasets, shown for grids  $\mathcal{G}$  that differ from  $\mathcal{G}_*$  by a single link  $(m, n)$ ; axes  $\times$  show connected nodes in  $\mathcal{G}_*$ ; (c) the distribution of probabilities for the transitions observed in data for the initial guess network  $\mathcal{G}_0$ ; (d) the distribution of probabilities for the transitions observed in data for the ground truth network  $\mathcal{G}_*$ ; (e) convergence of likelihood  $L(\mathcal{G})$  towards  $L(\mathcal{G}_*)$  in the optimisation process; average (solid lines)  $\pm$  one standard deviation (shaded areas) over the  $N_s = 42$  datasets; (f) convergence of network  $\mathcal{G}$  towards  $\mathcal{G}_*$ .

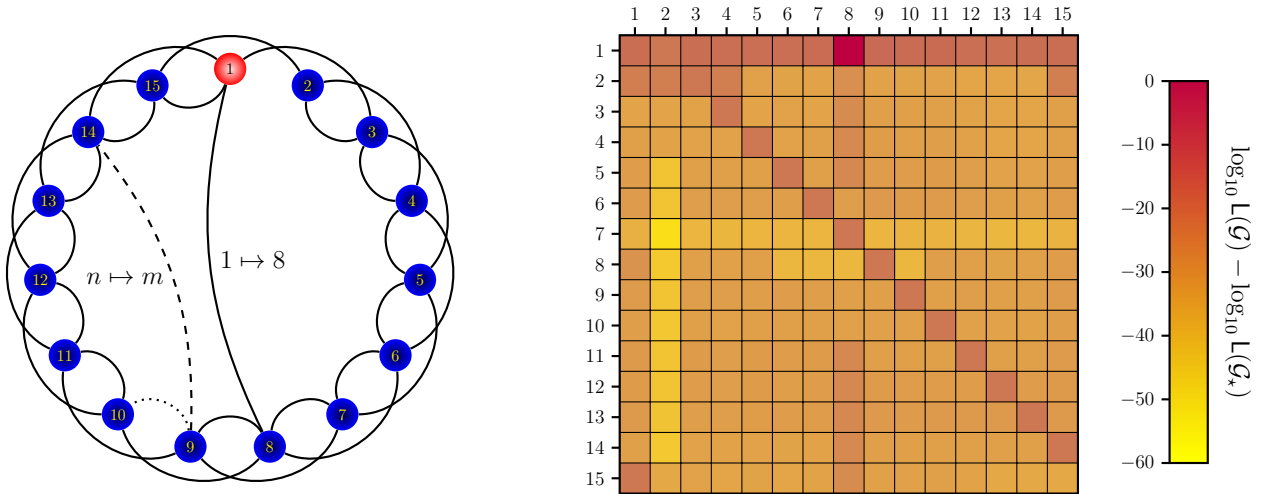


Figure 6: Inferring a rewired link in small world graph ( $N = 15$  nodes) from  $\varepsilon$ -SIS epidemic process with  $\beta = 1$ ,  $\gamma = 0.5$  and  $\varepsilon = 0.01$ : (left) the ground truth grid  $\mathcal{G}_*$  shown in its initial state; (right) the contrast  $\log_{10} L(\mathcal{G}) - \log_{10} L(\mathcal{G}_*)$  averaged over  $N_s = 42$  datasets, shown for grids  $\mathcal{G} \in \tilde{\mathcal{G}}$  from a class of small-world networks with a single rewired link.

of the contact network also contributed via higher TT ranks  $r \simeq 12.0 \pm 1.8$  for  $\mathcal{G} = \mathcal{G}_0$  and  $r \simeq 13.4 \pm 1.2$  for  $\mathcal{G} = \mathcal{G}_*$ . The total time required to perform the Bayesian optimisation with  $N_{\text{eval}} = 400$  steps of the MCMC algorithm took us about  $180 \cdot 10^3$  seconds, or just slightly over 2 days. For comparison, when SSA is used as the forward solver, one likelihood computation took CPU time  $\simeq 1292 \pm 58.7$  seconds for  $\mathcal{G} = \mathcal{G}_0$  and CPU time  $\simeq 853 \pm 24.4$  seconds for  $\mathcal{G} = \mathcal{G}_*$ .

From results shown in Fig. 5 we note that the convergence of both MCMC algorithms is stuck at a level where a small number of links of the network are inferred incorrectly, namely, approximately 5 of 36 links using the standard MCMC algorithm, and approximately 4 of 36 links using the MCMC algorithm without replacements. This highlights the potential of the no-replacement MCMC algorithm to tackle more complex problems, but also motivates the development of alternative approaches to black-box high-dimensional optimisation to improve their convergence and hence the quality of inference.

The fact that the MCMC algorithms got stuck before the ground state network is inferred can be explained by presence of local maxima in which the MCMC methods get trapped. This can be considered as a consequence of a too high contrast, that sharpens the high-dimensional landscape and makes both the global and local maxima steeper. If we use less data for Bayesian inference, the contrast reduces, making it easier for MCMC to escape from local optima by switching from current network  $\mathcal{G}_i$  to less attractive proposal  $\hat{\mathcal{G}}$  with probability  $L(\hat{\mathcal{G}})/L(\mathcal{G}_i) < 1$  as explained in Alg. 1. However, it also makes global maximum less emphasized and can lead to a situation where the optimal grid recovered by the Bayesian optimisation is not the same as the ground truth grid,  $\mathcal{G}_{\text{opt}} \neq \mathcal{G}_*$ .

### 3.3 Small world network

We note that even though the use of tensor product algorithms allows us to compute likelihoods (4) faster and more accurately, Bayesian inference of a contact network in a fully black-box setting remains a challenging task, as we see from experiments in Sec. 3.1 and Sec. 3.2.

In this section we present a preliminary experiment where we assume some prior knowledge of the contact network, which allows us to reduce the number of unknown parameters



even for a larger number of network nodes. Specifically, we assume that the contact network is from a family of small–world networks [74], which is shown in Figure 6(a). It consists of  $N = 15$  nodes which are arranged as a loop and connected with a double bond, where each node  $n \in \mathcal{V}$  is connected to nodes  $n + 1$  and  $n + 2$ , where we assume that indices go around the circle, so  $N + 1 = 1$  and  $N + 2 = 2$  when necessary. The main loop is rewired, i.e. a certain link  $(n, n + 1)$  is removed and replaced with a link  $(n, m)$  to a random node  $m \in \mathcal{V}$ , which provides additional connectivity. For this experiment we assumed that the ground truth network  $\mathcal{G}_*$  contains a single rewired link  $1 \mapsto 8$ , i.e. the link  $(1, 2)$  is removed and replaced with  $(1, 8)$ . We then proceed to infer this network, assuming that we know it is from the set of small–world networks with a single rewired link  $n \mapsto m$ , which we denote  $\tilde{\mathcal{G}}$ . The problem therefore reduces to finding only two parameters,  $n$  and  $m$ , and the search space shrinks from  $|\mathcal{G}| = 2^{N(N-1)/2}$  to only  $|\tilde{\mathcal{G}}| = N^2$  possible grids.

Inferring a network from a known class can be formulated as Bayesian optimisation (4) on a class of networks  $\tilde{\mathcal{G}}$  parametrised by small number of parameters. This removes our main computational challenge related to high dimensionality of the search space and allows us to solve this problem directly. We generated  $N_s = 42$  data samples by simulating the  $\varepsilon$ –SIS epidemic on a ground truth contact network  $\mathcal{G}_*$  using parameters  $\beta = 1$ ,  $\gamma = 0.5$  and  $\varepsilon = 0.01$ , for the duration of  $T = 1000$  time units, and re-sampled the data to a uniform grid with the time step  $\tau = 0.1$ , hence creating  $K = 10^4$  records for each data sample. Using tAMEn algorithm to model the evolution of epidemic on 15–node networks, we were able to compute the likelihoods for all grids  $\mathcal{G} \in \tilde{\mathcal{G}}$ . We then computed the average contrast for all  $\mathcal{G} \in \tilde{\mathcal{G}}$  as shown in Fig. 6(b). The results show that  $E[\log_{10} L(\mathcal{G}) - \log_{10} L(\mathcal{G}_*)] \leq -10$  for all  $\mathcal{G} \neq \mathcal{G}_*$ , which ensures that the ground truth network is a unique global maximum of the Bayesian optimisation problem (4).

## 4 Discussion

Inferring the contact network in a Bayesian optimisation framework requires us to estimate the likelihood of observed data  $\mathcal{X}$ , which are a realisation of epidemic dynamics on the ground truth network  $\mathcal{G}_*$ , to appear for the epidemic on another network  $\mathcal{G}$ . In a black–box setting, we have no a priori information on the network, and start the optimisation from an initial guess  $\mathcal{G}_0$  that may be (very) different from  $\mathcal{G}_*$ . For the grids  $\mathcal{G}$  in the vicinity of  $\mathcal{G}_0$ , observing the same dynamics as on  $\mathcal{G}_*$  is a (very) rare event, which we need to estimate with sufficient precision in order to evaluate the likelihoods  $L(\mathcal{G})$ . The slow convergence of the SSA algorithm limits its capability to recover rare events. By replacing it with the tensor product algorithms, we are able to recover rare events much more accurately by solving the forward problem in the CME form (10) and overcoming the curse of dimensionality. This allows the MCMC method to find its way from the initial network  $\mathcal{G}_0$  towards the optimum.

As the optimisation gets closer to  $\mathcal{G}_*$ , the likelihoods increase and the presence of steep local maxima slows down the convergence towards the global one. In this area high contrast ratios  $L(\mathcal{G}_*)/L(\mathcal{G})$  are undesirable as they make it harder for the MCMC algorithm to get out of local maxima. This can be addressed by using only a part of the available data to compute likelihoods (4) and/or tempering of  $L(\mathcal{G})$  to simplify the high–dimensional landscape for the optimisation. This has been used successfully for sampling from concentrated distributions of continuous random variables [14].

We also explored the potential of tensor product algorithms for tackling the network likelihood optimisation. However, these attempts so far were less efficient than the MCMC algorithm (in particular the MCMC without replacement). The TT-Cross algorithm [61] and its extensions [20] are used to compute a TT approximation to a black-box tensor by drawing a few adaptive samples from it using the maximum volume algorithm [32] or a greedy version

thereof [20]. These maximum volume samples are expected to be good candidates for the maximum absolute value of the tensor [32, 68]. However, the maximum volume algorithm requires all elements of a TT core, which must be drawn as full columns from the tensor, including elements which are known to be far from the maximum. MCMC probes only one element at a time, and can skip such unnecessary calculations. In numerical experiments with the linear chain, MCMC was systematically faster and more accurate compared to the TT-Cross maximizer, albeit by a modest margin (1-2 contacts). Tempering the likelihood to reduce its TT ranks and caching its values (which are often repeated in the TT-Cross) may make this approach faster in terms of the actual CPU time.

Another tensor optimiser proposed recently is PROTES [7], a probabilistic method similar to genetic algorithms. In each iteration, this algorithm draws  $K$  candidate optima as random samples from a probability distribution function in the TT format, which is in turn updated by a stochastic gradient ascent maximizing the probability of drawing  $k$  samples with the largest values of the sought function out of the  $K$  candidates. The default parameters proposed in [7] are  $k = 10$  and  $K = 100$ . Compared to our budget of  $N_{\text{eval}} = 400$  function evaluations, this corresponds to only 4 stochastic gradient ascent iterations, which are clearly insufficient and produce an almost random network. Taking  $K$  in the order of 10 (and hence  $k$  below 10) is uncompetitive too, since a few tens of iterations cannot compensate for a more random stochastic gradient due to a smaller  $k$ . However, it may be reasonable to use such an algorithm to fine-tune a previous TT approximation of the likelihood to new data.

## References

- [1] M. A. ACHTERBERG, B. PRASSE, AND P. VAN MIEGHEM, *Analysis of continuous-time markovian  $\varepsilon$ -sis epidemics on networks*, Phys. Rev. E, 105 (2022), p. 054305.
- [2] A. AMMAR, E. CUETO, AND F. CHINESTA, *Reduction of the chemical master equation for gene regulatory networks using proper generalized decompositions*, Int. J. Numer. Meth. Biomed. Engng., 28 (2012), pp. 960–973.
- [3] D. F. ANDERSON AND D. J. HIGHAM, *Multilevel Monte Carlo for continuous time Markov chains, with applications in biochemical kinetics*, Multiscale Modeling & Simulation, 10 (2012), pp. 146–179.
- [4] J. BALLANI AND L. GRASEDYCK, *Tree adaptive approximation in the hierarchical tensor format*, SIAM J. Sci. Comput., 36 (2014), pp. A1415–A1431.
- [5] G. BARCZA, O. LEGEZA, K. H. MARTI, AND M. REIHER, *Quantum-information analysis of electronic states of different molecular structures*, Phys. Rev. A, 83 (2011), p. 012508.
- [6] S. T. BARNARD, A. POTHEN, AND H. D. SIMON, *A spectral algorithm for envelope reduction of sparse matrices*, in Proc. ACM/IEEE Conference on Supercomputing, 1993, pp. 493–502.
- [7] A. BATSHEVA, A. CHERTKOV, G. RYZHAKOV, AND I. OSELEDETS, *PROTES: probabilistic optimization with tensor sampling*, arXiv preprint 2301.12162, 2023.
- [8] G. E. P. BOX AND G. C. TIAO, *Bayesian inference in statistical analysis*, Wiley, 1973.
- [9] T. BRITTON AND P. TRAPMAN, *Inferring global network properties from egocentric data with applications to epidemics*, Mathematical Medicine and Biology: A Journal of the IMA, 32 (2015), pp. 101–114.

- [10] I. BRUGERE, B. GALLAGHER, AND T. Y. BERGER-WOLF, *Network structure inference, a survey: motivations, methods, and applications*, ACM Comput. Surv., 51 (2018), pp. 24:1–24:39.
- [11] Y. CAO, A. TEREBUS, AND J. LIANG, *State space truncation with quantified errors for accurate solutions to discrete chemical master equation*, Bulletin of Mathematical Biology, 78 (2016), pp. 617–661.
- [12] J. D. CAROLL AND J. J. CHANG, *Analysis of individual differences in multidimensional scaling via  $n$ -way generalization of Eckart–Young decomposition*, Psychometrika, 35 (1970), pp. 283–319.
- [13] W.-Y. CHEN AND S. BOKKA, *Stochastic modeling of nonlinear epidemiology*, Journal of Theoretical Biology, 234 (2005), pp. 455–470.
- [14] T. CUI AND S. DOLGOV, *Deep composition of Tensor-Trains using squared inverse Rosenblatt transports*, Found. Comput. Math., 22 (2022), pp. 1863–1922.
- [15] T. CUI, S. DOLGOV, AND O. ZAHM, *Scalable conditional deep inverse rosenblatt transports using tensor trains and gradient-based dimension reduction*, Journal of Computational Physics, 485 (2023), p. 112103.
- [16] R. DE SMET AND K. MARCHAL, *Advantages and limitations of current network inference methods*, Nature Reviews Microbiology, 8 (2010), pp. 717–729.
- [17] F. DI LAURO, J.-C. CROIX, M. DASHTI, L. BERTHOUBE, AND I. Z. KISS, *Network inference from population-level observation of epidemics*, Scientific Reports, 10 (2020), p. 18779.
- [18] T. DINH AND R. B. SIDJE, *An adaptive solution to the chemical master equation using quantized tensor trains with sliding windows*, Physical Biology, 17 (2020), p. 065014.
- [19] S. DOLGOV AND B. KHOROMSKIY, *Simultaneous state-time approximation of the chemical master equation using tensor product formats*, Numer. Linear Algebra Appl., 22 (2015), pp. 197–219.
- [20] S. DOLGOV AND D. SAVOSTYANOV, *Parallel cross interpolation for high-precision calculation of high-dimensional integrals*, Comp. Phys. Comm., 246 (2020), p. 106869.
- [21] S. DOLGOV AND D. SAVOSTYANOV, *Tensor product approach to modelling epidemics on networks*, Applied Mathematics and Computation, 460 (2024), p. 128290.
- [22] S. V. DOLGOV, *A tensor decomposition algorithm for large ODEs with conservation laws*, Computational Methods in Applied Mathematics, 19 (2019), pp. 23–38.
- [23] S. V. DOLGOV AND D. V. SAVOSTYANOV, *Alternating minimal energy methods for linear systems in higher dimensions*, SIAM J. Sci. Comput., 36 (2014), pp. A2248–A2271.
- [24] A. ECONOMOU, A. GÓMEZ-CORRAL, AND M. LÓPEZ-GARCÍA, *A stochastic sis epidemic model with heterogeneous contacts*, Physica A, 421 (2015), pp. 78–97.
- [25] G. ENCISO, R. ERBAN, AND J. KIM, *Identifiability of stochastically modelled reaction networks*, European Journal of Applied Mathematics, 32 (2021), p. 865–887.
- [26] M. FIEDLER, *Algebraic connectivity of graphs*, Czechoslovak Mathematical Journal, 23 (1973), pp. 298–305.

- [27] ———, *A property of eigenvectors of nonnegative symmetric matrices and its application to graph theory*, Czechoslovak Mathematical Journal, 25 (1975), pp. 619–633.
- [28] P. GELSS, S. MATERA, AND C. SCHÜTTE, *Solving the master equation without kinetic Monte Carlo: Tensor train approximations for a CO oxidation model*, Journal of Computational Physics, 314 (2016), pp. 489–502.
- [29] D. T. GILLESPIE, *A general method for numerically simulating the stochastic time evolution of coupled chemical reactions*, J Comput. Phys., 22 (1976), pp. 403–434.
- [30] ———, *Approximate accelerated stochastic simulation of chemically reacting systems*, The Journal of Chemical Physics, 115 (2001), pp. 1716–1733.
- [31] J. P. GLEESON, *High-accuracy approximation of binary-state dynamics on networks*, Phys. Rev. Lett., 107 (2011), p. 068701.
- [32] S. A. GOREINOV, I. V. OSELEDETS, D. V. SAVOSTYANOV, E. E. TYRTYSHNIKOV, AND N. L. ZAMARASHKIN, *How to find a good submatrix*, in Matrix Methods: Theory, Algorithms, Applications, V. Olshevsky and E. Tyrtyshnikov, eds., World Scientific, Hackensack, NY, 2010, pp. 247–256.
- [33] C. GROENDYKE, D. WELCH, AND D. R. HUNTER, *Bayesian inference for contact networks given epidemic data*, Scand. J. Stat., 38 (2011), pp. 600–616.
- [34] A. GUPTA, C. SCHWAB, AND M. KHAMMASH, *DeepCME: A deep learning framework for computing solution statistics of the chemical master equation*, PLoS Comput Biol, 17 (2021), p. e1009623.
- [35] X. HAN, Z. SHEN, W.-X. WANG, AND Z. DI, *Robust reconstruction of complex networks from sparse data*, Phys. Rev. Lett., 114 (2015), p. 028701.
- [36] R. A. HARSHMAN, *Foundations of the PARAFAC procedure: models and conditions for an explanatory multimodal factor analysis*, UCLA Working Papers in Phonetics, 16 (1970), pp. 1–84.
- [37] M. HEGLAND, C. BURDEN, L. SANTOSO, S. MACNAMARA, AND H. BOOTH, *A solver for the stochastic master equation applied to gene regulatory networks*, Journal of Computational and Applied Mathematics, 205 (2007), pp. 708 – 724.
- [38] M. HEGLAND AND J. GARCKE, *On the numerical solution of the chemical master equation with sums of rank one tensors*, ANZIAM, 52 (2011), pp. C628–C643.
- [39] M. HEMBERG AND M. BARAHONA, *Perfect sampling of the master equation for gene regulatory networks*, Biophysical journal, 93 (2007), pp. 401–410.
- [40] A. L. HILL, D. G. RAND, M. A. NOWAK, AND N. A. CHRISTAKIS, *Emotions as infectious diseases in a large social network: the SISa model*, Proc. Royal Society B, 277 (2010).
- [41] F. L. HITCHCOCK, *The expression of a tensor or a polyadic as a sum of products*, J. Math. Phys, 6 (1927), pp. 164–189.
- [42] I. G. ION, C. WILDNER, D. LOUKREZIS, H. KOEPL, AND H. DE GERSEM, *Tensor-train approximation of the chemical master equation and its application for parameter inference*, The Journal of Chemical Physics, 155 (2021), p. 034102.

- [43] T. JAHNKE, *An adaptive wavelet method for the chemical master equation*, SIAM J. Sci. Comput., 31 (2010), p. 4373.
- [44] T. JAHNKE AND W. HUISINGA, *A dynamical low-rank approach to the chemical master equation*, Bulletin of Mathematical Biology, 70 (2008), pp. 2283–2302.
- [45] V. KAZEEV, M. KHAMMASH, M. NIP, AND C. SCHWAB, *Direct solution of the Chemical Master Equation using Quantized Tensor Trains*, PLOS Computational Biology, 10 (2014), p. e100359.
- [46] M. J. KEELING, *The effects of local spatial structure on epidemiological invasions*, Proc Biol Sci, 266 (1999), pp. 859–867.
- [47] M. J. KEELING AND K. T. EAMES, *Networks and epidemic models*, Interface, 2 (2005), pp. 295–307.
- [48] W. O. KERMACK AND A. G. MCKENDRICK, *A contribution to the mathematical theory of epidemics*, Proceedings of the Royal Society London A, 115 (1927), pp. 700–721.
- [49] I. Z. KISS, J. C. MILLER, AND P. L. SIMON, *Mathematics of Epidemics on Networks: From Exact to Approximate Models*, Springer, Berlin, 2017.
- [50] I. KRYVEN, S. RÖBLITZ, AND C. SCHÜTTE, *Solution of the chemical master equation by radial basis functions approximation with interface tracking*, BMC Systems Biology, 9 (2015), p. 67.
- [51] C. LESTER, R. E. BAKER, M. B. GILES, AND C. A. YATES, *Extending the multi-level method for the simulation of stochastic biological systems*, Bulletin of Mathematical Biology, 78 (2016), pp. 1640–1677.
- [52] J. LINDQUIST, J. MA, P. VAN DEN DRIESSCHE, AND F. H. WILLEBOORDSE, *Effective degree network disease models*, J Math Biol, 62 (2011), pp. 143–164.
- [53] A. Y. LOKHOV, M. MÉZARD, H. OHTA, AND L. ZDEBOROVÁ, *Inferring the origin of an epidemic with a dynamic message-passing algorithm*, Phys. Rev. E, 90 (2014), p. 012801.
- [54] W. MERBIS, C. DE MULATIER, AND P. CORBOZ, *Efficient simulations of epidemic models with tensor networks: Application to the one-dimensional susceptible-infected-susceptible model*, Phys Rev E, 108 (2023), p. 024303.
- [55] B. MICHEL AND A. NOUY, *Learning with tree tensor networks: Complexity estimates and model selection*, Bernoulli, 28 (2022), pp. 910 – 936.
- [56] J. C. MILLER, A. C. SLIM, AND E. M. VOLZ, *Edge-based compartmental modelling for infectious disease spread*, J. R. Soc. Interface, 9 (2012), p. 890–906.
- [57] S. MUKHERJEE AND T. P. SPEED, *Network inference using informative priors*, Proceedings of National Academy of Sciences, 105 (2008), pp. 14313–14318.
- [58] B. MUNSKY AND M. KHAMMASH, *The finite state projection algorithm for the solution of the chemical master equation*, The Journal of chemical physics, 124 (2006), p. 044104.
- [59] P. D. O’NEILL AND G. O. ROBERTS, *Bayesian inference for partially observed stochastic epidemics*, J. R. Statist. Soc. A, 162 (1999), p. 121–129.
- [60] I. V. OSELEDETS, *Tensor-train decomposition*, SIAM J. Sci. Comput., 33 (2011), pp. 2295–2317.

- [61] I. V. OSELEDETS AND E. E. TYRTYSHNIKOV, *TT-cross approximation for multidimensional arrays*, Linear Algebra Appl., 432 (2010), pp. 70–88.
- [62] R. PASTOR-SATORRAS, C. CASTELLANO, P. VAN MIEGHEM, AND A. VESPIGNANI, *Epidemic processes in complex networks*, Rev. Modern Phys., 87 (2015), p. 925.
- [63] D. A. RAND, *Correlation equations and pair approximations for spatial ecologies*, in Advanced Ecological Theory: Principles and Applications, Blackwell Science, Oxford, 1999, ch. 4, pp. 100–142.
- [64] G. O. ROBERTS AND J. S. ROSENTHAL, *Quantitative non-geometric convergence bounds for independence samplers*, Methodol. Comput. Appl. Probab., 13 (2011), pp. 391–403.
- [65] P. B. ROHRBACH, S. DOLGOV, L. GRASEDYCK, AND R. SCHEICHL, *Rank bounds for approximating Gaussian densities in the Tensor-Train format*, SIAM/ASA Journal on Uncertainty Quantification, 10 (2022), pp. 1191–1224.
- [66] U. SCHOLLWÖCK, *The density-matrix renormalization group in the age of matrix product states*, Annals of Physics, 326 (2011), pp. 96–192.
- [67] R. SHAH AND D. P. KROESE, *Without-replacement sampling for particle methods on finite state spaces*, Statistics and Computing, 28 (2018), pp. 633–652.
- [68] K. SOZYKIN, A. CHERTKOV, R. SCHUTSKI, A.-H. PHAN, A. S. CICHOCKI, AND I. OSELEDETS, *TTOpt: A maximum volume quantized tensor train-based optimization and its application to reinforcement learning*, in Advances in Neural Information Processing Systems, vol. 35, 2022, pp. 26052–26065.
- [69] A. SUKYS, K. ÖCAL, AND R. GRIMA, *Approximating solutions of the chemical master equation using neural networks*, iScience, 25 (2022), p. 105010.
- [70] M. TAYLOR, T. J. TAYLOR, AND I. Z. KISS, *Epidemic threshold and control in a dynamic network*, Phys. Rev. E, 85 (2012), p. 016103.
- [71] N. G. VAN KAMPEN, *Stochastic processes in physics and chemistry*, North Holland, Amsterdam, 1981.
- [72] P. VAN MIEGHEM AND E. CATOR, *Epidemics in networks with nodal self-infection and the epidemic threshold*, Phys. Rev. E, 86 (2012), p. 016116.
- [73] H. D. VO AND R. B. SIDJE, *An adaptive solution to the chemical master equation using tensors*, The Journal of Chemical Physics, 147 (2017), p. 044102.
- [74] D. J. WATTS AND S. H. STROGATZ, *Collective dynamics of ‘small-world’ networks*, Nature, 393 (1998), pp. 440–442.
- [75] M. YOUSSEF AND C. SCOGGIO, *An individual-based approach to SIR epidemics in contact networks*, Journal of Theoretical Biology, 283 (2011), pp. 136–144.
- [76] J. ZHANG, J. M. F. MOURA, AND J. ZHANG, *Contact process with exogenous infection and the scaled SIS process*, Journal of Complex Networks, 5 (2017), p. 712–733.